Dispersing Perylene Diimide/SWCNT Hybrids: Structural Insights at the Molecular Level and Fabricating Advanced Materials

9 AUTHORS, INCLUDING:

Yael Tsarfati
Weizmann Institute of Science
1 PUBLICATION   0 CITATIONS

SEE PROFILE

Elisha Krieg
Harvard Medical School
11 PUBLICATIONS   264 CITATIONS

SEE PROFILE

Eyal Shimoni
Weizmann Institute of Science
61 PUBLICATIONS   1,948 CITATIONS

SEE PROFILE

Jonathan Baram
Weizmann Institute of Science
9 PUBLICATIONS   183 CITATIONS

SEE PROFILE

Dispersing Perylene Diimide/SWCNT Hybrids: Structural Insights at the Molecular Level and Fabricating Advanced Materials

Yael Tsarfati,[†] Volker Strauss,[§] Susanne Kuhri,[§] Elisha Krieg,[†] Haim Weissman,[†] Eyal Shimoni,[‡] Jonathan Baram,[†] Dirk M. Guldi,*[,§] and Boris Rybtchinski*[,†]

[†]Department of Organic Chemistry, and [‡]Department of Chemical Research Support, the Weizmann Institute of Science, Rehovot 76100, Israel

[§]Department of Chemistry and Pharmacy & Interdisciplinary Center for Molecular Materials (ICMM), Friedrich-Alexander-Universität Erlangen-Nürnberg, Egerlandstrasse 3, 91058 Erlangen, Germany

ⓢ *Supporting Information*

ABSTRACT: The unique properties of carbon nanotubes (CNT) are advantageous for emerging applications. Yet, the CNT insolubility hampers their potential. Approaches based on covalent and noncovalent methodologies have been tested to realize stable dispersions of CNTs. Noncovalent approaches are of particular interest as they preserve the CNT's structures and properties. We report on hybrids, in which perylene diimide (PDI) amphiphiles are noncovalently immobilized onto single wall carbon nanotubes (SWCNT). The resulting hybrids were dispersed and exfoliated both in water and organic solvents in the presence of two different PDI derivatives, **PP2b** and **PP3a**. The dispersions were investigated using cryogenic transmission electron microscopy (cryo-TEM), providing unique structural insights into the exfoliation. A helical arrangement of **PP2b** assemblies on SWCNTs dominates in aqueous dispersions, while a single layer of **PP2b** and **PP3a** was found on SWCNTs in organic dispersions. The dispersions were probed by steady-state and time-resolved spectroscopies, revealing appreciable charge redistribution in the ground state, and an efficient electron transfer from SWCNTs to PDIs in the excited state. We also fabricated hybrid materials from the **PP2b**/SWCNT dispersions. A supramolecular membrane was prepared from aqueous dispersions and used for size-selective separation of gold nanoparticles. Hybrid buckypaper films were prepared from the organic dispersions. In the latter, high conductivity results from enhanced electronic communication and favorable morphology within the hybrid material. Our findings shed light onto SWCNT/dispersant molecular interactions, and introduce a versatile approach toward universal solution processing of SWCNT-based materials.
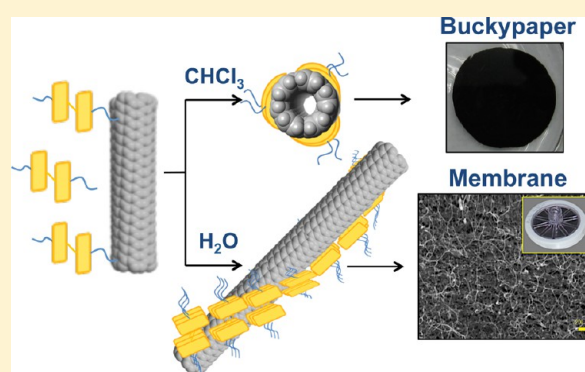
INTRODUCTION

Research in the area of carbon nanotubes has been thriving over the past decade. The unique one-dimensional structure of carbon nanotubes (CNTs) enables their outstanding electronic, thermal, and mechanical properties, rendering them unrivaled by any other class of molecules.[1] For example, CNTs have exceptional mechanical properties, with significant potential for applications in reinforcing composite materials.[2] Other promising applications of CNTs are found in the field of nanoelectronics.[3,4] Despite the great potentials, none of the proposed CNT applications have so far come through. One of the main reasons is the insolubility of CNTs in common solvents, including water and most organics. Notably, CNTs are typically found in the form of bundles held together by strong intertubular van der Waals interactions, 0.5 eV/μm between individual CNTs.[1] As such, it is desirable to explore ways to individualize, disperse, and stabilize CNTs in various media, and to understand the underlying chemistry.

To overcome the attractive forces between individual CNTs and improve their solubilization, *covalent functionalization* has emerged as a versatile strategy.[5−9] Despite the success in optimizing the solubility of CNTs in a wide range of solvents, chemical functionalization, that is, modifying the sp^2 carbon framework, alters their intrinsic electronic and mechanical properties.[1] Driven by such drawbacks, *noncovalent functionalization* by means of polymer wrapping,[10,11] interacting with biomolecules such as DNA[12,13] and peptides,[14] and adsorbing ionic or nonionic surfactants[15−18] has been the strategy of choice en-route CNT solubilization. It allows preservation of the intrinsic electronic and mechanical properties of CNTs, in general, and the charge transport over several micrometers, in particular. The *noncovalent functionalization* provides efficient means to solubilize CNTs via the formation of micellar structures with CNTs at their core.[18]

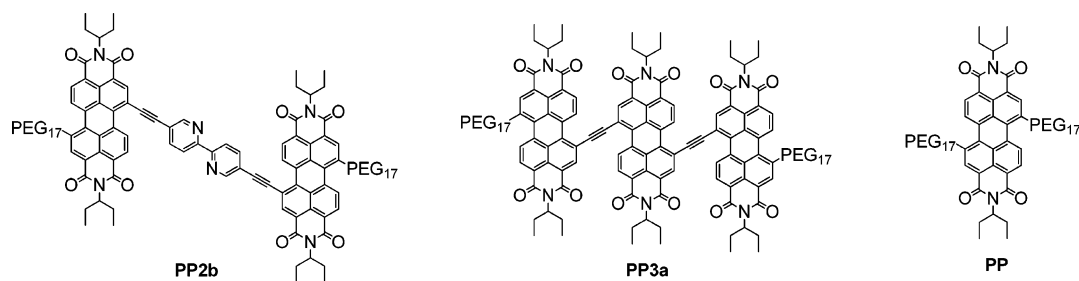**Figure 1.** PDI-based dispersant molecules: **PP2b**, **PP3a**, and **PP**. $PEG_{17} = -(O-CH_2-CH_2)_{17}-OMe$.

To attain aqueous CNT dispersions, a plethora of ionic or nonionic surfactants have been investigated. Typically, they are classified according to the nature of their head groups.[19] First, the most broadly used surfactants are anionic, including sodium dodecyl sulfonate (SDS), sodium dodecyl sulfate (SDBS), etc. Second, there are cationic surfactants such as dodecyltrimethylammonium bromide (DTAB), and nonionic surfactants such as polyoxyethylenes.

In addition, polycyclic aromatic amphiphiles based on perylenes,[20] pyrenes,[9,19,21−24] etc. have been shown to individualize, disperse, and stabilize CNTs in aqueous media. In these particular cases, the strong and specific interactions with CNTs rely on hydrophobic, $\pi-\pi$ stacking and charge transfer forces, whereas the solubility in water stems from the hydrophilic groups covalently attached to the aromatic backbones of the dispersants.

Several groups have studied the self-assembly of amphiphilic building blocks based on perylene-3,4,9,10-tetra-carboxylic acid diimides (PDIs) as the hydrophobic core in aqueous media.[25,26] PDI is a well-studied and widely utilized molecular building block, since it has excellent optical and electronic properties, thermal and photochemical stability, strong absorption in the visible part of the solar spectrum, and high fluorescence quantum yields.[25,27] For example, Hirsch et al. have reported on PDIs that enable the realization of stable CNT dispersions in water. They have specifically addressed the correlation between the PDI substitutions and the dispersion efficiency.[1,20,28−31] Electron donor−acceptor hybrids based on PDIs and CNTs have been studied by Guldi et al. in aqueous media.[32] In these hybrids, PDIs serve as electron acceptors, while CNTs function as electron donors, yielding a unidirectional electron transfer from CNTs to PDIs.

Compared to water as a medium, work related to surfactant-assisted dispersions in organic solvents is rather scarce.[33] Generally, CNTs are colloidally dispersible in organic solvents such as o-dichlorobenzene (ODCB), N-methylpyrrolidinone (NMP), N,N-dimethylformamide (DMF), and N,N-dimethylacetamide (DMAc). However, the resulting dispersions feature either limited stability over time[9] or bundling[10,11] in the absence of surfactants.[34] To the best of our knowledge, stable dispersions in organic solvents have so far only been achieved using polymers.[5,9−11] For example, poly(phenylacetylene) was found to wrap around CNTs rendering them soluble in common organic solvents.[9]

In this contribution, we demonstrate that PDIs with an extended PDI core and PEG substituents efficiently disperse and stabilize SWCNTs in both aqueous and organic solutions. To the best of our knowledge, this is the first time that SWCNTs were dispersed in an organic solvent ($CHCl_3$) noncovalently using a small organic molecule. The structure of the resulting hybrids was investigated by cryo-TEM with emphasis on the molecular morphology. Excellent electronic interactions in the hybrids result in ground state doping, enabling efficient communication not only in the ground state, but also in the excited state. Furthermore, we demonstrated the versatility and applicability of the PDI/SWCNT dispersions with respect to fabrication of two different hybrid materials: a supramolecular membrane for size-selective nanoparticle separations (from aqueous dispersion) and a conductive film ("buckypaper"), from organic dispersion. The ability to create a universal organic and aqueous dispersion system may significantly expand the existing toolbox for fabricating CNT-based materials.

■ RESULTS AND DISCUSSION

Dispersions of Hybrid Systems. Regarding solubility and functionality of SWCNT-based nanohybrids, molecular systems featuring a multi-PDI conjugated core and PEG substituents can be especially advantageous.[35] The former leads to strong interactions between the aromatic core and SWCNTs, and the latter provides enhanced solubility in organic and aqueous media. To achieve SWCNT dispersions, we utilized two PEG—PDI systems with extended flat cores, namely **PP2b** with a di-PDI core connected by ethynyl bipyridine linker and **PP3a** having a PDI trimer connected by ethynyl linkers (Figure 1).[36,37] As a reference we used **PP**, a PDI monomer, endowed with two hydrophilic PEG_{17} chains (Figure 1).

Dispersion Procedure. In a typical dispersion procedure, 1 mL of chloroform was added to a vial with **PP2b** or **PP3a** and (6,5)-SWCNTs in a weight (wt) ratio of 5:1, respectively. The resulting mixture (10^{-4} M, PDI dispersant concentration) was then tip-sonicated for 5 min and centrifuged to remove excess of undispersed SWCNTs. These conditions were found to be optimal in terms of dispersion stability and SWCNT exfoliation as well as its structural integrity (Figure 2); see Experimental Section and Supporting Information for details. The dispersion aptitudes were assessed by absorption and fluorescence spectroscopy. In the absorption spectra, the (6,5)-SWCNT feature at 997 nm, which arises upon sonication with **PP2b** or **PP3a**, prompts their exfoliation by the latter (Figure 2b,d).[38] Notably, the absorption is red-shifted relative to the 975 nm maximum of (6,5)-SWCNTs, which were dispersed with electronically inactive surfactants.[39] In the fluorescence spectra, quenching of the **PP2b** fluorescence (Figure 2c,e) indicates electronic communication between **PP2b** and SWCNTs due to $\pi-\pi$ stacking interactions.[1,22,23,40] Remarkably, procedures involving 10 min of 15kg centrifugation after sonication resulted in chloroform dispersions, which were stable for months, while the reported stabilities for CNT dispersions in organic solvents usually range from hours to days.[8,9]

Microscopic Characterization. To investigate the structure of the hybrid systems and to estimate the exfoliation efficiency
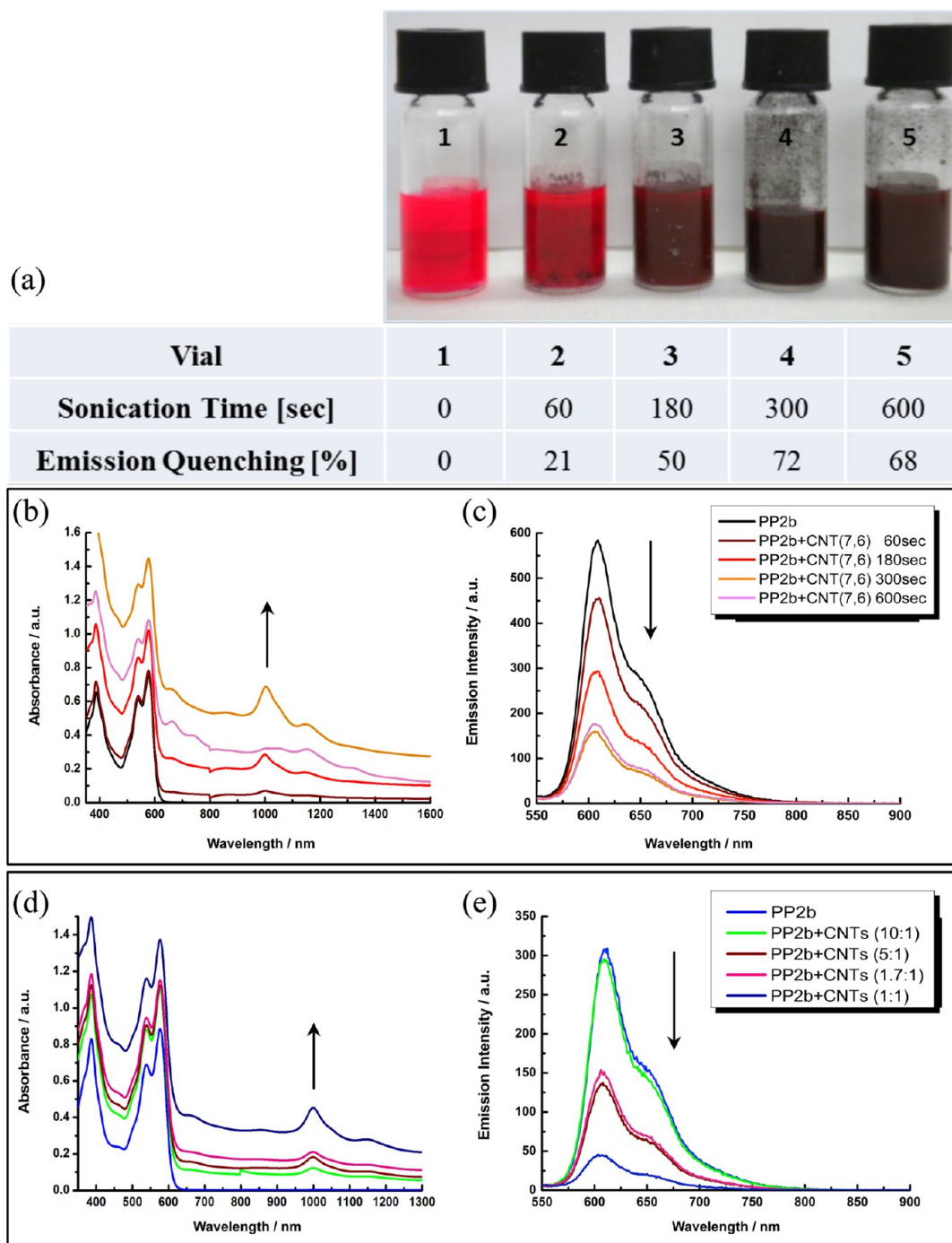
Figure 2. Optimization of **PP2b**/SWCNT chloroform dispersion. (a) A photograph of the dispersions after varying sonication times, according to the table. (b and c) Absorption and emission spectra of the dispersions depicted in (a). (d and e) Absorption and emission spectra of dispersions upon varying wt ratio of **PP2b** to CNTs.

of SWCNTs, we employed cryo-TEM imaging. In the case of **PP2b**/SWCNT chloroform dispersions, cryo-TEM[41] images reveal SWCNTs dispersed in the vitrified solution (Figure 3a). Furthermore, images, which were taken after sublimating chloroform, revealed clusters of aligned SWCNTs with average distances of 1.7 nm between neighboring SWNCTs (see inset in Figure 3b and FFT in the Supporting Information, Figure S6). The distances between adjacent SWCNTs are 0.8–0.9 nm, a value consient with the size of a stack of two **PP2b**'s between adjacent SWCNTs (Figure 3c,d; see also Supporting Information). From the latter we conclude that a mono-

molecular layer of **PP2b**, which is immobilized onto SWCNTs via π−π stacking, is sufficient to exfoliate them.

Possible structures of the **PP2b**/SWCNT hybrids were modeled using molecular mechanics (Figure 4). On the basis of the cryo-TEM images, we postulate a model that is best described as **PP2b** wrapping SWCNTs via π−π interactions creating a monolayer, where three **PP2b** molecules cover a SWCNT segment, ca. 4 nm in length. Independent confirmation for this model came from thermogravimetric (TGA) measurements on **PP2b**/SWCNT films (see Supporting Information). The latter reveals a **PP2b**/SWCNT ratio
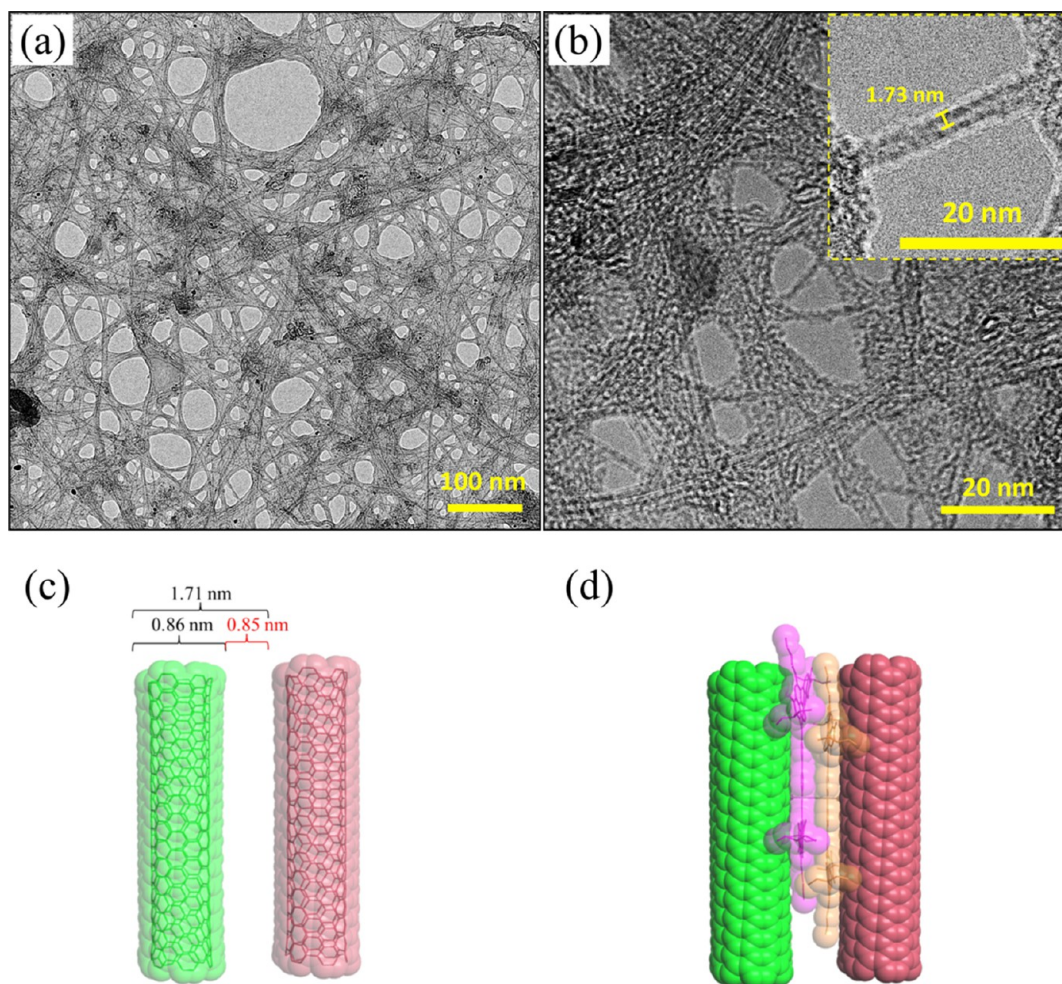
Figure 3. (a) A representative cryo-TEM image of **PP2b**/SWCNTs in chloroform dispersion. (b) Higher magnification image, taken after subliming chloroform (gray amorphous material is excess of **PP2b**). Inset: an example of two adjacent SWCNTs. (c) A model of two adjacent SWCNTs, showing averaged distances: between the SWCNTs (1.71 nm), diameter (0.86 nm), and the distance between the sidewalls (0.85 nm). (d) A model showing the arrangement of two **PP2b** molecules between the adjacent SWCNTs.
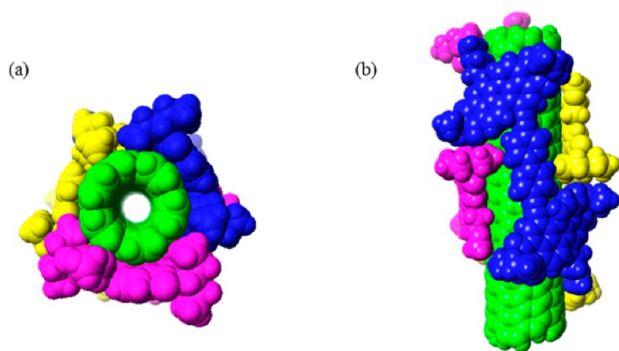

Figure 4. A model of **PP2b**/SWCNT, in a space-filling representation: (6,5) SWCNT (green); **PP2b** molecules (with one PEG unit) are in blue, yellow, and pink; (a) cross-section; (b) side view.

compatible with the model depicted in Figure 4. **PP3a**/SWCNT hybrid in chloroform exhibits a similar mode of interactions, as revealed by cryo-TEM images (Supporting Information Figures S4 and S5).

Physicochemical Characterization. The organic dispersions were further characterized by photophysical techniques. We envisaged that the contact between the PDI cores of **PP2b** and **PP3a**, and SWCNTs, as well as the electron donor−acceptor character of **PP2b**/SWCNT and **PP3a**/SWCNT hybrids, would result in strong electronic interactions. To minimize the excess of free **PP2b** and **PP3a**, which may obscure the photophysics of the hybrids, the organic dispersions were further optimized in terms of **PP2b**/SWCNT and **PP3a**/SWCNT hybrid enrichment (see Supporting Information).

Raman spectroscopy provided sound indication for chirality selectivity and strong electronic interactions. All of the spectra were recorded upon 1064 nm excitation, baseline corrected, and normalized with respect to the G$^+$-band. Figure 5 presents the normalized radial breathing mode (RBM) and G-band regions for **PP2b**/SWCNT, **PP3a**/SWCNT, and pristine SWCNT.[42] A comparison of the spectra with and without PDIs reveals up-shifts of the respective G$^+$-bands (Figure 5, inset), which is indicative of shifting charge density from the PDIs to SWCNTs.[43] Notably, in the case of **PP3a**/SWCNT, the shift toward higher frequencies is appreciably stronger. Furthermore, drastic intensity variations were observed in the RBM-bands. For example, RBMs at 261, 311, and 331 cm^{-1} correlate with (7,6)-, (6,5)-, and (6,4)-SWCNTs, respectively.[42] In the presence of **PP2b** and **PP3a**, the intensity of the 261 cm^{-1} RBM increases, while a decrease is observed for the 311 and 331 cm^{-1} RBMs. The effect was more pronounced in the case of **PP3a**, indicating that the enrichment of (7,6)-SWCNTs
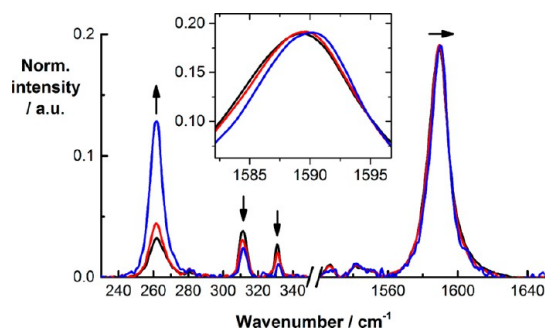
Figure 5. Normalized solid state Raman spectra (λ_{ex} = 1064 nm) of pristine SWCNTs (black), and enriched dispersions of **PP2b**/SWCNT (red), and **PP3a**/SWCNT (blue), showing the RBM and G regions (the latter is shown also in the inset).

in the presence of PDIs is apparently more significant in the case of **PP3a**. When turning to the D-band, representing defects within SWCNTs, no appreciable differences were observed when comparing sonicated and nonsonicated solutions.

As a complement, we probed the NIR photoluminescence of the **PP2b**/SWCNT and **PP3a**/SWCNT hybrids in chloroform. Notably, the 3D fluorescence spectra in the excitation range applicable to the investigations of SWCNTs were dominated by residual PDI fluorescence (Supporting Information Figure S19). Therefore, we focused on the SWCNT photoluminescence upon excitations at 575, 650, and 725 nm. Interestingly, we observed a broad emission peak at ~1210 nm with low intensities upon 650 and 725 nm excitation, where wavelengths where (7,5)- and (7,6)-SWCNTs are resonant. In Figure 6 and
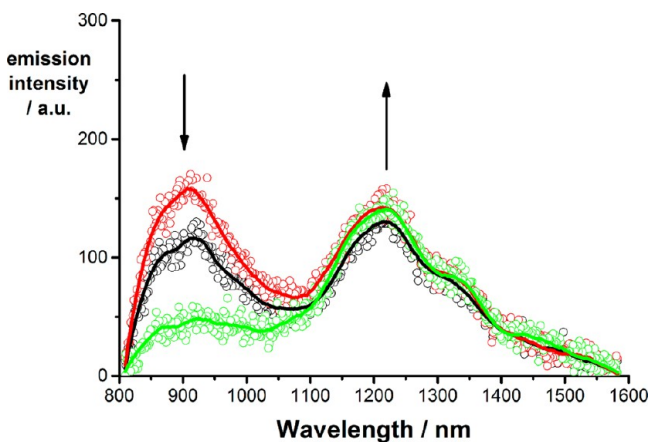

Figure 6. NIR emission spectra of **PP2b** upon sequential enrichment with SWCNTs in CHCl$_3$, excitation at 650 nm at room temperature. Arrows refer to the progression of the enrichment.

Supporting Information Figure S20, the evolution of the emission features upon addition of SWCNTs to solutions of **PP2b** and **PP3a**, respectively, are shown. In particular, the band peaking at around 910 nm, which originates from free **PP2b** or **PP3a**, decreases gradually when SWCNTs were added, while the peak at 1210 nm together with a shoulder at ~1310 nm grows in slightly. (7,5)- and (7,6)-SWCNTs are resonant with 650 nm excitation, typically showing photoluminescence maxima at ~1035 and ~1130 nm, respectively, when dispersed with electronically inactive surfactants.[44] With **PP2b** and **PP3a**, we observed the photoluminescence features at 1210 and 1310

nm, respectively, which imply shifts of 175 nm (0.18 eV). Strong changes in charge densities from SWCNTs to PDIs have been seen in the past to lead to similar spectroscopic signatures.[32] Characteristic charge transfer-induced shifts of the photoluminescence in n-doped SWCNTs are ~0.04 eV.[45,46] In addition, electrochemical and chemical doping of SWCNTs have evoked large shifts in the emission peaks, which have been attributed to the presence of trions.[47−53] The stability of trions in SWCNTs at room temperature has been analyzed on the basis of a tight-binding model.[54]

The photoactivity of **PP2b**/SWCNT and **PP3a**/SWCNT dispersions was further studied by femtosecond transient absorption (TA) spectroscopy. For **PP2b**/SWCNT, immediately upon 532 nm excitation, a set of transient minima evolves at 587, 667, and 1007 nm, accompanied by a set of maxima at 455, 490, 634, 880, and 1110 nm (Figure 7a). The minima at 667 and 1007 nm relate to the ground state S$_{22}$ and S$_{11}$ absorptions of (6,5)-SWCNTs, and the minimum at 578 nm corresponds to the PDI's ground state. The ground state recovery is biexponential with a short-lived component of 2.9 ps and long-lived component of 42 ps (Figure 7b). At the conclusion of the short-lived component, that is, approximately after 5 ps, the transients at 667 and 1007 nm are subject to blue shifts toward 660 and 1003 nm, respectively. In line with previous investigations, we assign these blue-shifted minima to oxidized SWCNTs.[55] In addition, transient maxima at 480, 680, and 890 nm correlate with the features of one electron-reduced **PP2b** as confirmed by spectroelectrochemical studies (see Supporting Information). Thus, the short- and long-lived components are likely to relate to charge separation and charge recombination, respectively. It should be noted that additional long-lived transients at 600, 660, and 877 nm are stemming from **PP2b** that is not immobilized onto SWCNTs. Overall, the observed dynamics indicate a photoinduced electron transfer from SWCNT to **PP2b**.

A similar behavior was found for **PP3a**/SWCNT dispersions. A set of minima evolves immediately after photoexcitation. The minima at 661 and 1004 nm correspond to the ground state of (6,5)-SWCNTs, while the minimum at 578 nm mirror images the PDI's ground state (Figure 8a). The set of maxima at 445, 483, 675, 857, and 1110 nm are excited state transitions of **PP3a**. The ground state recovery evolves with two significant lifetimes of 4 and 40 ps. As observed in the case of **PP2b**/SWCNT, the transient minima at 661 and 1004 nm blue-shift throughout the initial 4 ps decay to 651 and 997 nm, respectively, corresponding to the oxidized SWCNTs.[55] The additional set of maxima at 670, 740, and 1120 nm are in sound agreement with the differential absorption changes noted in spectroelectrochemical reduction experiments with **PP3a** (see Supporting Information). Hence, the observed dynamics are consistent with an electron transfer from SWCNT to **PP3a** upon photoexcitation.

The charge separation lifetimes are 3 and 4 ps for **PP2b** and **PP3a**, respectively, and the ground state recovery via charge recombination occurs within about 40 ps for both hybrids. These values are in good agreement with the lifetimes found in other PDI/SWCNT hybrids.[55] Overall, SWCNTs evoke a rapid decay of the PDI singlet excited state leading to a fully charge separated state, that is, reduced PDIs and oxidized SWCNTs.

Aqueous Dispersion. In the next step, we investigated the ability of **PP2b** to disperse SWCNTs in aqueous solutions (see Experimental section and Supporting Information for details). Cryo-TEM images of **PP2b**/SWCNT in aqueous solutions
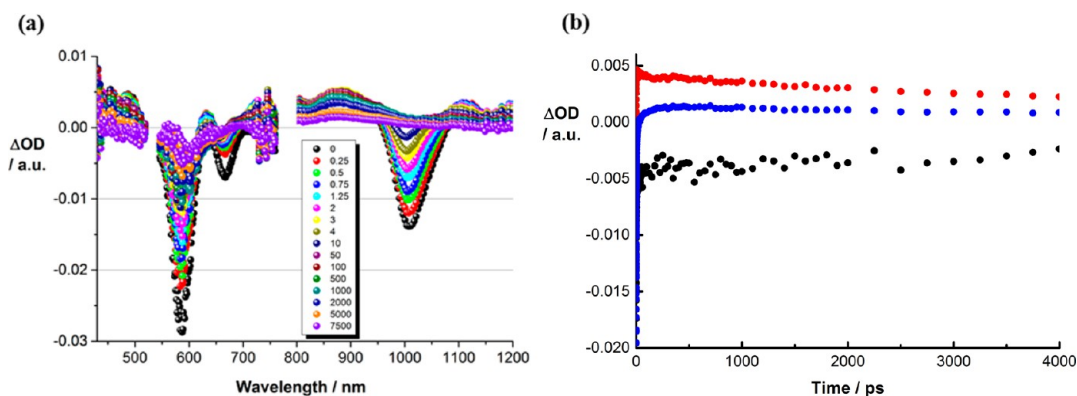
Figure 7. (a) Differential absorption spectra obtained upon femtosecond laser flash photolysis (532 nm) of **PP2b**/SWCNT with time delays between 0 and 7500 ps. (b) Corresponding time absorption profiles at 570 nm (black), 850 nm (red), and 1000 nm (blue).

Figure 8. (a) Differential absorption spectra obtained upon femtosecond excitation (532 nm) of **PP3a**/SWCNT with time delays between 0 and 7500 ps. (b) Corresponding time absorption profiles at 570 nm (black), 850 nm (red), and 1000 nm (blue).
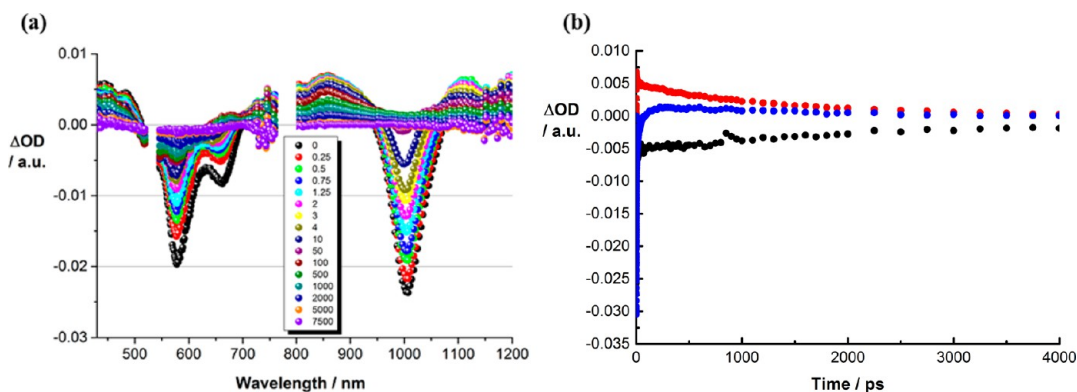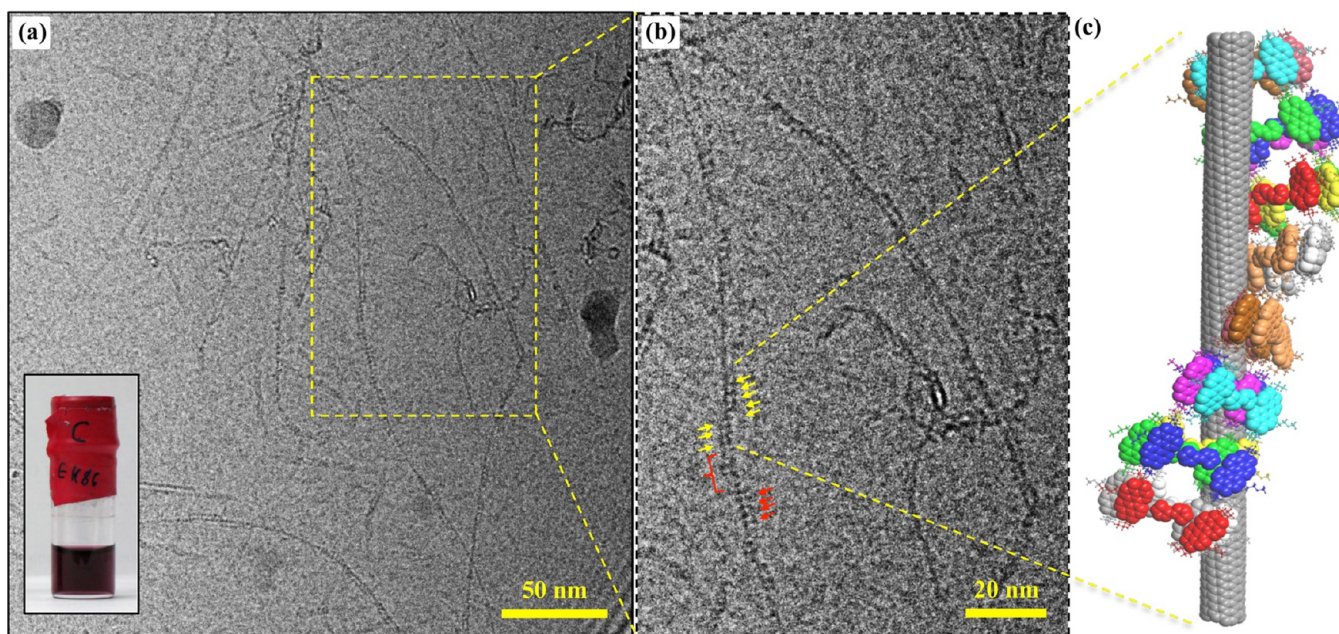

Figure 9. (a) A representative cryo-TEM image of **PP2b**/SWCNT in 20% THF/H$_2$O dispersion. The inset shows a photograph of the dispersion. (b) Magnified section of the image on the left. The arrows point at high contrast segments that are **PP2b** assemblies on the SWCNT scaffold. The yellow arrows point at the **PP2b** assemblies that construct half a pitch of a helical arrangement. The corresponding model is presented in (c). The red bracket marks a region where the helix is presumed to continue behind the SWCNT, reappearing as the high contrast segmented structure indicated by the red arrows. Deviations from such wrapping are also observed, with varying degrees of helicity and order. (c) A molecular model of **PP2b**/SWCNT in aqueous dispersion (optimized using MM2 and MM3 force fields).

revealed structural features different from those observed in chloroform dispersions. In particular, segmented structures, which are 3−4 nm in length and 1.8−2.2 nm in height, exhibiting a helical motif, were observed to uniformly cover SWCNTs (Figure 9). Such a pattern is presumably due to **PP2b** assemblies, as suggested by the molecular model best-fit to the cryo-TEM images (Figure 9c). Unlike in chloroform, where an excess of **PP2b** is solubilized, **PP2b** molecules should aggregate in aqueous solutions,[36] and their aggregation is likely to be dictated by SWCNTs.

To the best of our knowledge, high-resolution cryo-TEM images, providing insights into molecular details regarding SWCNT interactions with dispersants, are rare. A notable exception is the case of SDS immobilized onto multiwalled carbon nanotubes (MWCNT),[56] for which a helical organization, comparable to our findings, was observed. Importantly, our cryo-TEM images of organic and aqueous dispersions revealed significant differences in molecular organization on SWCNTs.

Hybrid Materials. *Membranes for Size-Selective Separations.* We have previously demonstrated that aqueous assemblies of **PP2b** represent a unique platform for the fabrication of supramolecular ultrafiltration membranes.[57,58] Hence, we probed the suitability of aqueous **PP2b**/SWCNT dispersions to form hybrid membranes upon deposition. The membrane was fabricated by filtrating 2.5 mL of an aqueous dispersion (10^{-4} M **PP2b**; 5:1 **PP2b**/SWCNT wt ratio, in THF/H$_2$O, 1:4, v/v) over a cellulose acetate (CA) filter in a controlled pressure setup (Figure 10). The filtration resulted in a colorless filtrate and a deposition of the hybrid on the CA support (Figure 10c,e−f).
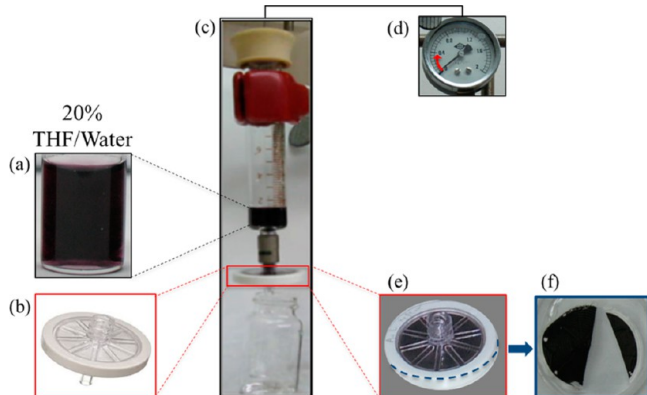

Figure 10. **PP2b**/SWCNT hybrid supramolecular membrane fabrication. (a) Aqueous dispersion solution is filtered at a transmembrane pressure of 0.4 bar (d) over a CA support (b). The filtrate was colorless and a deposited layer was formed on the CA support (e), opened and cut membrane is shown in (f).

The hybrid deposit was investigated using cryogenic scanning electron microscopy (cryo-SEM). Cross-sectional images showed a homogeneous 3−4 µm layer of the hybrid material on top of the CA support (Figure 11a). A sharp and defined interface between the coarse CA and the smooth **PP2b**/SWCNT layer indicates that the latter does not penetrate appreciably into the CA pores (Figure 11b). SWCNTs appear in the images as thin curved white threads, indicating excellent exfoliation, and **PP2b** appears as the porous gray background, in which the SWCNTs are embedded (Figure 11c).

Two control experiments were conducted to assess the role of **PP2b** in the formation of the hybrid membrane. In the first control experiment, we aimed at fabricating the membrane in the absence of surfactants. The resulting deposit was characterized by cryo-SEM (see Supporting Information, Figure S21). Expectedly, lacking an adequate medium for SWCNTs, the deposition resulted in a noncontinuous and heterogeneous SWCNT layer, where SWCNT aggregates were nonhomogeneously spread over the CA support.

In the second control, Brij-96V, a standard SWCNT surfactant, was used (Figure 12c, see Experimental Section). The **Brij**/SWCNT deposit showed resemblance to the **PP2b**/SWCNT membrane, a continuous membrane on top of the CA support, with a sharp interface between the two. However, the membrane's thickness was not uniform, ranging from 0.5 to 3 µm (Figure 12c,d). Furthermore, aggregates of SWCNT bundles were observed (Figure 12d) at the interface of the membrane and the support. Thus, a membrane much inferior to **PP2b**/SWCNT was formed. Notably, **PP2b** supramolecular fibers not only function as a solubilizing agent, but also provide a structural scaffold that improves the quality of fabricated hybrid membranes.

To study the **PP2b**/SWCNT hybrid membrane performance, filtration experiments were carried out. Gold nanoparticles (NP) with different size distributions were filtered through the hybrid membrane and were characterized by TEM prior and after filtration (Figure 13 and Supporting Information Figure S22). The cutoff for filtration experiments, which is defined as a size larger than 99% of the particles in the filtrate, was found to be 7 nm (Figure 13d,e), a cutoff slightly larger than the 5 nm found for **PP2b**-based membranes.[57] The **PP2b**/SWCNT hybrid membrane has a potential to be more robust than a **PP2b** membrane previously reported by us,[57] due to the SWCNTs embedding. Accordingly, very thin hybrid membranes (3−4 µm-thick) showed excellent performance in nanoparticle separations.

Hybrid Conductive Film. Devices based on macroscopic arrays of SWCNTs such as yarns and films are of interest due to their advantageous electronic properties.[59] In this respect, strong electronic coupling in **PP2b**/SWCNT hybrids might be beneficial for the preparation of conductive films, so-called "buckypaper" (BP). BP fabrication follows a simple bottom up approach, in which a suspension of SWCNTs is filtered through a support filter.

We performed solution-based fabrication of **PP2b**−BP utilizing **PP2b**/SWCNT chloroform dispersions (Figure 14), which were filtered through a polyvinylidene fluoride (PVDF) filter in a pressure-controlled setup. The film was then washed with chloroform to remove excess **PP2b**. The PVDF support with the deposited **PP2b**/SWCNT film was transferred into an acetone solution, immediately releasing the film from the support. The free-standing **PP2b**/SWCNT film can be deposited onto a solid support such as silicon wafer or glass slide. As a control, a BP film was also fabricated from **Brij**/SWCNT aqueous dispersion. Notably, we were unable to fully delaminate the **Brij**/SWCNT deposit, and only small fragments of the **Brij**/SWCNT films were released and used for further analysis.

TGA and cyclic voltammetry were performed in order to study the hybrid BP composition. TGA revealed the presence of surfactants as indicated by additional peaks appearing for **PP2b**−BP and **Brij**−BP when compared to the TGA analysis of SWCNTs (see Supporting Information). Cyclic voltam-
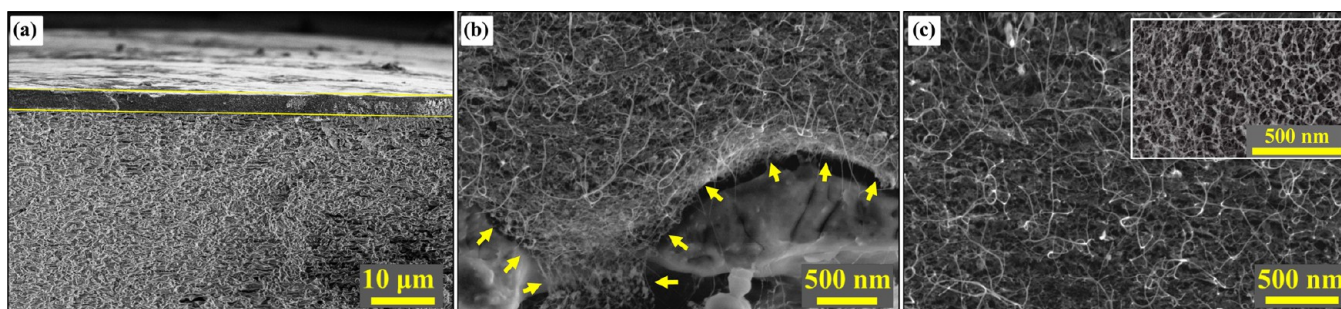
Figure 11. Cryo-SEM cross-section images of a **PP2b**/SWCNT membrane. (a) The membrane on the top of the CA support (3–4 μm thickness) is marked in yellow. (b) A magnified image of (a) showing the sharp border, marked by arrows, between the membrane in and the CA support. (c) SWCNTs appear as curved white strings embedded in the porous **PP2b**. Inset: **PP2b** membrane without SWCNTs.[57]
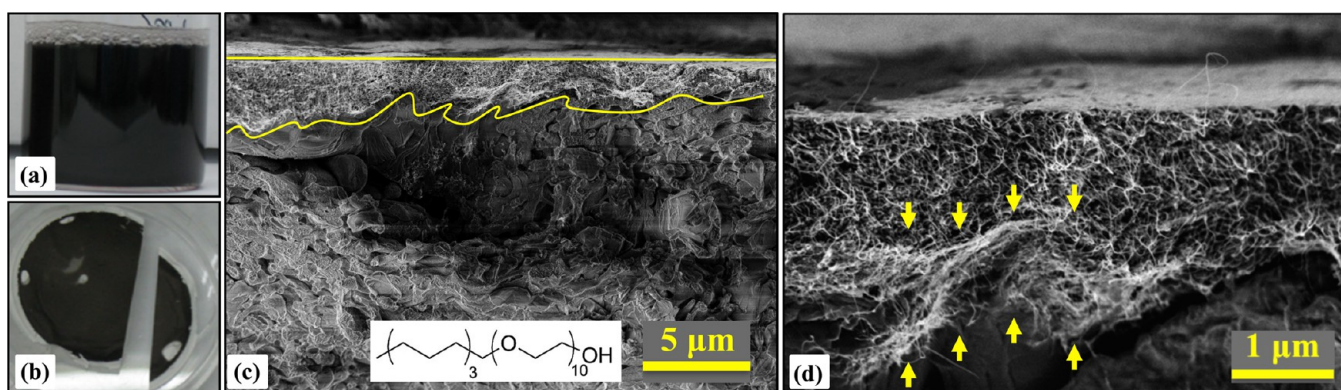

Figure 12. Cryo-SEM cross-section images of a **Brij**/SWCNT membrane. (a) A photograph of the **Brij**/SWCNTs dispersion solution. (b) A photograph of the deposited **Brij**/SWCNT hybrid membrane. (c) Between the yellow lines, the deposited **Brij**/SWCNT hybrid membrane on the CA support. (d) A magnified image of the **Brij**/SWCNTs hybrid membrane. Aggregates of SWCNTs are indicated by arrows.
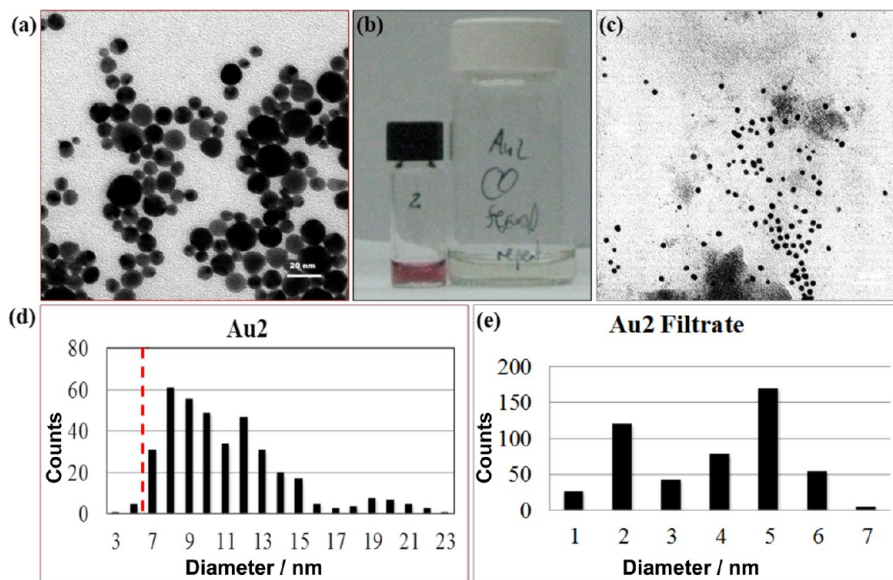

Figure 13. Filtration experiments: gold NP separations using a **PP2b**/SWCNT membrane. (a) A representative TEM image of Au2, gold NPs solution. (b) A photograph of the gold NP's solutions before the filtration (smaller vial on the left) and the filtrate (bigger vial on the right). (c) A representative TEM image of Au2 gold NPs filtrate. (d and e) Histograms displaying the NPs distribution.

metric reduction attributed to **PP2b** was observed for **PP2b–BP,** and no significant reduction peak was detected in the case of **Brij–BP** (see Supporting Information). SEM revealed entangled networks of SWCNTs in both cases (Figure S23 in the Supporting Information).

The electrical characteristics of the films were investigated in inert atmosphere, using four point probe conductivity measurements. The films exhibited linear $I–V$ dependence, characteristic of an ohmic behavior. The measurements indicated that the conductivity of **PP2b–BP** is by one order of magnitude higher than that of **Brij–BP** (Figure 15).
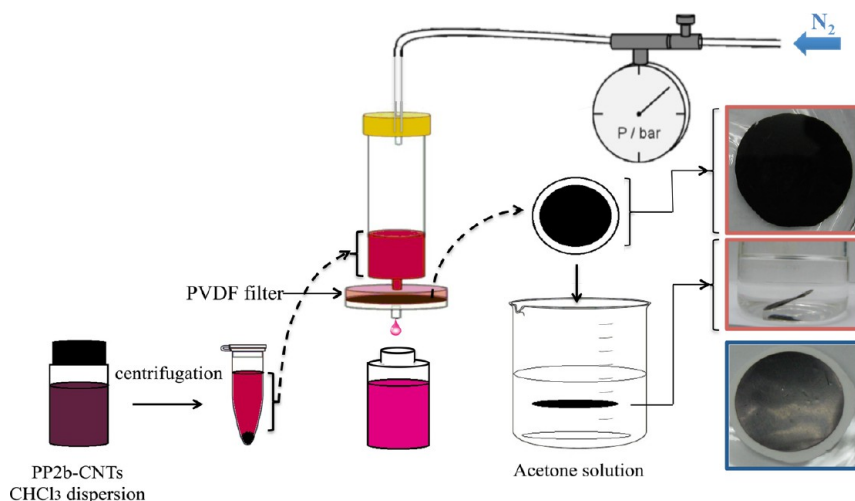
Figure 14. PP2b/SWCNT film fabrication process: **PP2b**/SWCNT chloroform dispersion solution is centrifuged. The supernatant is then filtered through a PVDF filter. A deposit is formed on the filter and immersed into an acetone solution to be released as a film. (a) **PP2b**/SWCNT film on the PVDF filter. (b) Released **PP2b**/SWCNT film floating in acetone solution. (c) **Brij**/SWCNT film on PVDF filter.
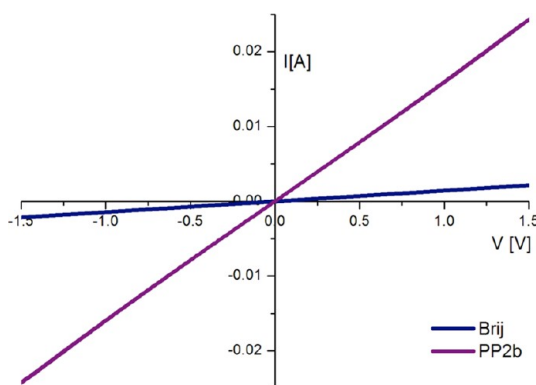

Figure 15. An $I-V$ curve of the buckypapers.

PP2b−BP showed a resistance of tens of Ohms, while in **Brij−BP** it is hundreds of Ohms. AFM measurements enabled us to determine the film thicknesses of 630 nm for **PP2b−BP** and 850 nm for **Brij−BP**, which allowed assessing the resistivity. The resistivity of **PP2b−BP**, 0.01−0.02 $[\Omega\cdot\text{cm}]$, indicates good conductivity,[60−64] superior to that of **Brij−BP**, ~0.2 $[\Omega\cdot\text{cm}]$, by about one order of magnitude. To the best of our knowledge, most commonly used surfactants in BP preparation are electronically inactive and, hence, lower the film's conductivity. In stark contrast, an electron-accepting surfactant such as **PP2b** offers an alternative. To this end, our studies in this contribution, including fluorescence, Raman, transient absorption spectroscopies, conductivity measurements, as well as the literature data,[32] point to strong electronic communication between SWCNTs and the immobilized PDI to result in an enhanced p-type character of SWCNTs. Equally important are the structural properties of the **PP2b−BP** hybrid, ensuring that the interactions between **PP2b** and SWCNTs are uniform over short and long-range.

■ CONCLUSIONS

We have demonstrated that **PEG−PDI** amphiphiles assist in the efficient exfoliation and dispersion of SWCNTs in both organic and aqueous solutions. This is, *to the best of our knowledge*, the first time that stable SWCNT dispersions were obtained in chloroform and imaged by cryo-TEM. Cryo-TEM images of **PP2b**/SWCNT and **PP3a**/SWCNT hybrids enable unique insights regarding the supramolecular structure of SWCNTs wrapped by PDIs. Thus, a single layer of PDIs is sufficient to individualize SWCNT in the case of chloroform. In aqueous medium, helical arrangements of **PP2b** assemblies are immobilized onto SWCNTs by virtue of hydrophobic and $\pi-\pi$ stacking interactions. The latter translates in the ground state into strong electronic communications between PDIs and SWCNTs leading to a charge transfer state with a sizable redistribution of charge density. Considering the electron accepting properties of PDIs, the latter enhances the p-type character of SWCNTs. In the excited state, a rapid electron transfer from SWCNTs to PDIs affords a fully charge separated state. Corroboration for the electron transfer came from a number of complementary photophysical measurements, in general, and transient absorption measurements, in particular.

We have further demonstrated the utility and versatility of **PP2b**/SWCNT dispersions in terms of fabricating hybrid materials. First, a supramolecular membrane was prepared from the aqueous dispersions. Second, a hybrid conducting bucky-paper film was prepared from the organic dispersions. The membrane was characterized by cryo-SEM, confirming its hybrid structure, in which SWCNTs are embedded within the porous **PP2b** supramolecular structure. The membrane was applicable for gold NPs size separation and may be further developed to allow tunable cutoff, higher flow rate, and enhanced robustness. The buckypaper film was straightforwardly fabricated from organic dispersions and showed promising electrical properties, in which the interplay between electronic and morphological factors plays a decisive role.

Overall, **PP2b**/SWCNT dispersions enable simple fabrication of CNT-based materials due to their universality (organic and aqueous medium), and good electronic communications between the dispersing PDIs and SWCNTs. Molecular-level structural characterization of the PDI/SWCNT hybrids allow a rare insight into the exfoliation propensities, and show, for the first time, that a monomolecular layer of the dispersant is sufficient for SWCNT individualization and solubilization.

■ EXPERIMENTAL SECTION

General. SWCNTs were obtained from Sigma-Aldrich and used as received. Purified CoMoCAT-Single-Wall Carbon Nanotubes SG-65, carbon >90%, ≥77% (carbon as SWNT), 0.7−0.9 nm diameter (by fluorescence) and Chirality distribution: >50% (6,5). The synthesis of the PDI derivatives have been published elsewhere[36,37] and **PP** was obtained as a side product of **PP2b** synthesis.

Cryo-TEM was performed using a Tecnai F20 transmission electron microscope operating at 200 kV and using a Gatan 626 cooling holder and transfer station with a TVIPS F415 CCD digital camera, or a Tecnai T12 transmission electron microscope operated at 120 kV, using a Gatan 626 cooling holder and transfer station, with a TVIPS F415 CCD digital camera.

Aqueous Sample Preparation. A total of 6.5 μL of the sample was applied on a 300-mesh copper grid coated with lacey carbon (Pacific Grid-Tech supplies). Samples were blotted in an environment at 25 °C and 100% relative humidity, and subsequently plunged into liquid ethane using a using Leica EM-GP Automatic Grid Plunger and were equilibrated at −178 °C in the microscope prior to imaging.

Organic Solvent Sample-Preparation for TEM and Cryo-TEM. A total of 6.5 μL of sample was applied on a 200-mesh copper grid coated with holey carbon (Pacific Grid-Tech supplies). The samples were blotted at 24 °C in a CEVS manual grid plunger that was saturated with chloroform vapor, and then plunged into liquid nitrogen. The specimens were equilibrated at −178 °C in the microscope prior to the imaging process. Later, the samples were warmed slowly to −110 °C allowing sublimation of the chloroform from the grid. Imaging performed thereafter was performed at room temperature.

Cryo-SEM sample preparation involved the high pressure freezing (HPF) technique. For this purpose, membranes were cut using a razor blade to fit in an aluminum disc (outer diameter 3.0 mm, thickness 0.5 mm, inner diameter 2.0 mm, cavity depth 0.15 mm). Hexadecene was used for filling empty spaces in order to prevent collapse of the disc under the applied high pressure (2100 bar). A flat disc covered the disc containing the sample. HPF was carried out using a Bal-Tec HPM 010. Subsequently, the frozen sample was released from the disc under liquid nitrogen, clamped vertically using a special holder and transferred into BAF 060 (Leica Microsystems, Vienna, Austria) freeze etching system where it was fractured with a precooled razor blade. Solvent was allowed to sublime (−105 °C, 1 h). The sample was then transferred to an Ultra 55 cryo-SEM (Zeiss) using the VCT 100 cryo-transfer holder and was observed at an acceleration voltage of 1−2.5 kV using the in-lens detector.

TEM was performed on a Philips T12 transmission electron microscope operated at 120 kV and equipped with a TVIPS F224HD CCD digital camera. A total of 2.5 μL of the sample was applied to a grid after 1 min under glowing discharge and dried in air. The used grids were 200-mesh copper grids (Pacific Grid Tech supplies) precoated with Formvar carbon film and 300-mesh copper grids (Pacific Grid Tech supplies) precoated with holey thin carbon film. The images of nanoparticles were analyzed using iTEM. For creation of particles' size histograms, the grids where scanned and for each a statistics was made using 4−5 representative images of the grid.

SEM for buckypaper surface morphology was performed on (1) Zeiss Supra 55VP FE-SEM. It is equipped with EDS (Oxford Instruments), CL, ET, AsB (angle selective backscattered) and InLens detectors. (2) Zeiss Ultra 55 FE-SEM. It is equipped with ET, EsB (energy selective backscattered) and InLens detectors. It has a cryo-stage - Leica (formerly BAl-Tec AG, Liechtenstein). All samples were deposited on a piece of silicon wafer and the imaging was operated at 3−5 kV.

UV/vis absorption and fluorescence measurements were carried out on a Cary-5000 spectrometer (Varian) and a Cary Eclipse fluorimeter (Varian), respectively. For fluorescence measurements, the excitation/emission geometry was right angle.

MALDI-TOF mass spectrometry was carried out using a AB SCIEX 5800 MALDI TOF/TOF System Equipped with Nd:YAG (355 nm) laser with 1 kHz pulse.

Femtosecond transient absorption spectroscopy was carried out using a mode-locked Ti:sapphire laser CPA-2101 (Clark-MXR, Inc.) in connection with a Helios transient absorption pump/probe (Ultrafast systems). The excitation wavelength of 532 nm was achieved by means of noncollinear optical parametric amplification of the fundamental laser beam.

Raman spectra were recorded using a FT-Raman RFS 100 system (Bruker) with a Ge-detector using a 1064 nm using a Nd:YAG laser for excitation.

AFM was used to measure the buckypaper thickness, employing NT-MDT NTEGRA instrument, using the Smena (tip scanning) head operated in semicontact mode. The cantilever probe was Olympus AC240 with nominal 70 kHz frequency. Amplitude set point ratio was approximately 0.9. Images were line-leveled using the manufacturer software and heights measured using cross-sectional profiles and by distance between peaks of histograms of surface heights taken over a region including both upper and lower part of a step.

Electrochemical experiments were carried out using a CHI660A electrochemical workstation; ITO glass substrates (7 mm × 50 mm × 0.7 mm) served as a working electrode, Ag/Ag⁺ were used as reference electrodes, and a Pt wire was used as a counter electrode. TBAF (0.1 M) in dry ACN was used as a supporting electrolyte. All electrochemical measurements were performed under nitrogen/Argon atmosphere. The investigated films were deposited over the ITO and then CV was measured.

It should be noted that a significantly larger area of a film was measured for the **PP2b−BP** relatively to the **Brij−BP**, due to the technical problem of separation of the **Brij−BP** from the PVDF support.

TGA experiments were carried out using a thermal analyzer SDT Q 600.

Molecular modeling was carried out using Scigress Explorer Ultra (7.7.0.49). The CNT structure had been created by TubeGen. The models of **PP2b**/SWCNTs were optimized using sequential augmented MM2 and MM3 methods for energy minimizations.

Dispersions Preparation. In a typical dispersion experiment, a stock solution of SWCNTs was made of an immersion of raw SWCNTs in CHCl₃ using 3 min of bath sonication. The stock solution was used immediately after preparation. The **PDI**'s stock solutions were also prepared in CHCl₃. The required volumes were taken from the stock solutions, put together and dried in high vacuum. The solvent of the dispersion was then added and the mixture was tip-sonicated. The dispersion solutions were composed of 1×10^{-4} M **PDI** and 20 wt % of CNTs to **PDI**. They were prepared as 1 mL solutions using 5 min of tip sonication, or as 10 mL solution using 25 min of tip sonication (for the BPs fabrication). The dispersion solvents were CHCl₃ and 20% THF/H₂O.

Dispersions of **Brij**/SWCNT were also prepared as a control: SWCNT and Brij stock solutions were dried together followed by the addition of water, with 20 wt % of **Brij** to SWCNT ratio.

Hybrid Enrichment Procedure. SWCNTs/PDIs dispersions were prepared by a sequential enrichment process, in which 0.2 mg of PDI was dissolved in chloroform and 0.5 mg of (6,5)-SWCNTs was added stepwise to the solution. Each addition step was followed by 2 min of ultrasonication, centrifugation (15*kg*, 10 min) and spectroscopic analysis. These steps were repeated until no further spectroscopic changes were notable. The supernatant was used for further spectroscopic and microscopic analyses.

Membrane Preparation. In a typical experiment, 2.5 mL of **PP2b**/SWCNT aqueous dispersion solution (20% THF/H₂O, 1×10^{-4} M **PP2b**, 20 wt % of SWCNT to **PP2b**) was filtered over a CA syringe filter (Whatman Puradisc FP 30, CA; effective filtration area, 5.7 cm²; pore size, 0.45 mm). Care was taken to avoid the presence of air bubbles in the chamber, which would affect the formation of a homogeneous layer of supramolecular material. The filtrate solution was refiltered twice, making sure the filtrate is colorless (i.e., all the **PP2b** is retained in the membrane). The filter housing was kept filled with aqueous solvent and the supramolecular membrane was used directly for Cryo-SEM imaging.

Filtration Experiment. Following the membrane's preparation, 3 mL of aqueous solution containing gold nanoparticles (0.1 mM, capped with mercaptopropionic acid, pH 9), was filtered over the membrane at a constant transmembrane pressure of 0.4 bar to stabilize material packing and flow rate. The filter housing was kept filled with the aqueous solvent and then 3 mL of Au NPs solution was filtered over the supramolecular membrane at a constant pressure of 0.4 bar using controlled pressure setup. Filtrate (~3 mL) was collected after the dead volume of 1 mL solution passed through the filter housing. Subsequently, the filter was rinsed with about 6 mL of water (containing 0.1 mM nanoparticle capping agent at the pH of the nanoparticle solution). Six different size distributions of Au NPs solutions were used.

Buckypaper Preparation. *PP2b–BP.* The **PP2b**/SWCNT $CHCl_3$ dispersion solution was centrifuged for 20 min at $16kg$, and the supernatant was collected. The supernatant (~9 mL) was then filtered through a PVDF membrane, and washed with $CHCl_3$. A film was deposited on the PVDF support and immersed into acetone solution, resulting in an immediate release of the film from the membrane. The film was dried on air.

Brij–BP. A control BP was prepared from **Brij**/CNTs aqueous dispersion solution in the same manner. It should be noted that the film in this case was not released by the acetone solution. Only small pieces of the film were separated from the support, by heating the acetone solution used for the release.

Buckypaper Electrical Measurements. Buckypapers were fabricated and deposited on microscope slide. Then the resistance of the films was measured over several points and on different films, using four-point probe in an inert glovebox atmosphere.

■ ASSOCIATED CONTENT

Ⓢ Supporting Information

Cryo-TEM and SEM images, photophysical and TGA data, membrane filtration data, and molecular modeling data. The Supporting Information is available free of charge on the ACS Publications website at DOI: 10.1021/jacs.5b03167.

■ AUTHOR INFORMATION

Corresponding Authors

*boris.rybtchinski@weizmann.ac.il

*dirk.guldi@fau.de

Notes

The authors declare no competing financial interest.

■ ACKNOWLEDGMENTS

■ REFERENCES

(1) Backes, C.; Schmidt, C. D.; Hauke, F.; Böttcher, C.; Hirsch, A. *J. Am. Chem. Soc.* **2009**, *131*, 2172−2184.

(2) Dresselhaus, M. S.; Dresselhaus, G.; Jorio, A. *Annu. Rev. Mater. Res.* **2004**, *34*, 247−278.

(3) Endo, M.; Hayashi, T.; Kim, Y. A.; Terrones, M.; Dresselhaus, M. S. *Philos. Trans. R. Soc., A* **2004**, *362*, 2223−2238.

(4) Ding, L.; Zhang, Z.; Liang, S.; Pei, T.; Wang, S.; Li, Y.; Zhou, W.; Liu, J.; Peng, L. *Nat. Commun.* **2012**, *3*, 677.

(5) Hirsch, A. *Angew. Chem., Int. Ed.* **2002**, *41*, 1853−1859.

(6) Banerjee, S.; Kahn, M. G. C.; Wong, S. S. *Chem.—Eur. J.* **2003**, *9*, 1898−1908.

(7) Banerjee, S.; Hemraj-Benny, T.; Wong, S. S. *Adv. Mater.* **2005**, *17*, 17−29.

(8) Tasis, D.; Tagmatarchis, N.; Bianco, A.; Prato, M. *Chem. Rev.* **2006**, *106*, 1105−1136.

(9) Fujigaya, T.; Nakashima, N. *Polym. J.* **2008**, *40*, 577−589.

(10) Star, A.; Liu, Y.; Grant, K.; Ridvan, L.; Stoddart, J. F.; Steuerman, D. W.; Diehl, M. R.; Boukai, A.; Heath, J. R. *Macromolecules* **2003**, *36*, 553−560.

(11) Hwang, J.-Y.; Nish, A.; Doig, J.; Douven, S.; Chen, C.-W.; Chen, L.-C.; Nicholas, R. J. *J. Am. Chem. Soc.* **2008**, *130*, 3543−3553.

(12) Nakashima, N.; Okuzono, S.; Murakami, H.; Nakai, T.; Yoshikawa, K. *Chem. Lett.* **2003**, *32*, 456−457.

(13) Zheng, M.; Jagota, A.; Semke, E. D.; Diner, B. A.; McLean, R. S.; Lustig, S. R.; Richardson, R. E.; Tassi, N. G. *Nat. Mater.* **2003**, *2*, 338−342.

(14) Witus, L. S.; Rocha, J.-D. R.; Yuwono, V. M.; Paramonov, S. E.; Weisman, R. B.; Hartgerink, J. D. *J. Mater. Chem.* **2007**, *17*, 1909.

(15) Connell, M. J. O.; Bachilo, S. M.; Huffman, C. B.; Rialon, K. L.; Boul, P. J.; Noon, W. H.; O'Connell, M. J.; Moore, V. C.; Strano, M. S.; Haroz, E. H.; Kittrell, C.; Ma, J.; Hauge, R. H.; Weisman, R. B.; Smalley, R. E. *Science* **2002**, *297*, 593−596.

(16) Ishibashi, A.; Nakashima, N. *Chem.—Eur. J.* **2006**, *12*, 7595−7602.

(17) Ke, P. C. *Phys. Chem. Chem. Phys.* **2007**, *9*, 439−447.

(18) Wenseleers, W.; Vlasov, I. I.; Goovaerts, E.; Obraztsova, E. D.; Lobach, A. S.; Bouwen, A. *Adv. Funct. Mater.* **2004**, *14*, 1105−1112.

(19) Backes, C. *Noncovalent Functionalization of Carbon Nanotubes*; Springer Berlin Heidelberg: Berlin, Heidelberg, 2012.

(20) Backes, C.; Schmidt, C. D.; Hauke, F.; Hirsch, A. *Chem.—Asian J.* **2011**, *6*, 438−444.

(21) Backes, C.; Mundloch, U.; Ebel, A.; Hauke, F.; Hirsch, A. *Chem.—Eur. J.* **2010**, *16*, 3314−3317.

(22) Tomonari, Y.; Murakami, H.; Nakashima, N. *Chem.—Eur. J.* **2006**, *12*, 4027−4034.

(23) Ehli, C.; Rahman, G. M. A.; Jux, N.; Balbinot, D.; Guldi, D. M.; Paolucci, F.; Marcaccio, M.; Paolucci, D.; Melle-Franco, M.; Zerbetto, F.; Campidelli, S.; Prato, M.; Chemistry, O.; Ciamician, C. G.; Uni, V.; Selmi, V. F. *J. Am. Chem. Soc.* **2006**, *128*, 11222−11231.

(24) Sgobba, V.; Troeger, A.; Cagnoli, R.; Mateo-Alonso, A.; Prato, M.; Parenti, F.; Mucci, A.; Schenetti, L.; Guldi, D. M. *J. Mater. Chem.* **2009**, *19*, 4319.

(25) Krieg, E.; Rybtchinski, B. *Chem.—Eur. J.* **2011**, *17*, 9016−9026.

(26) Rybtchinski, B. *ACS Nano* **2011**, *5*, 6791−6818.

(27) Langhals, H. *Helv. Chim. Acta* **2005**, *88*, 1309−1343.

(28) Backes, C.; Hauke, F.; Hirsch, A. *Adv. Mater.* **2011**, *23*, 2588−2601.

(29) Backes, C.; Mundloch, U.; Schmidt, C. D.; Coleman, J. N.; Wohlleben, W.; Hauke, F.; Hirsch, A. *Chem.—Eur. J.* **2010**, *16*, 13185−13192.

(30) Englert, J. M.; Rohrl, J.; Schmidt, C. D.; Graupner, R.; Hundhausen, M.; Hauke, F.; Hirsch, A. *Adv. Mater.* **2009**, *21*, 4265−4269.

(31) Backes, C.; Hauke, F.; Schmidt, C. D.; Hirsch, A. *Chem. Commun.* **2009**, *7345*, 2643−2645.

(32) Ehli, C.; Oelsner, C.; Guldi, D. M. D.; Mateo-alonso, A.; Prato, M.; Schmidt, C.; Backes, C.; Hauke, F.; Hirsch, A. *Nat. Chem.* **2009**, *1*, 243−249.

(33) Vaisman, L.; Wagner, H. D.; Marom, G. *Adv. Colloid Interface Sci.* **2006**, *128−130*, 37−46.

(34) Nguyen, T. T.; Nguyen, S. U.; Phuong, D. T.; Nguyen, D. C.; Mai, A. T. *Adv. Nat. Sci. Nanosci. Nanotechnol.* **2011**, *2*, 035015.

(35) Görl, D.; Zhang, X.; Würthner, F. *Angew. Chem., Int. Ed.* **2012**, *51*, 6328−6348.

(36) Krieg, E.; Shirman, E.; Weissman, H.; Shimoni, E.; Wolf, S. G.; Pinkas, I.; Rybtchinski, B. *J. Am. Chem. Soc.* **2009**, *131*, 14365−14373.

(37) Shahar, C.; Baram, J.; Tidhar, Y.; Weissman, H.; Cohen, S. R.; Pinkas, I.; Rybtchinski, B. *ACS Nano* **2013**, *7*, 3547−3556.

(38) Tan, Y.; Resasco, D. E. *J. Phys. Chem. B* **2005**, *109*, 14454−14460.

(39) Bachilo, S. M.; Strano, M. S.; Kittrell, C.; Hauge, R. H.; Smalley, R. E.; Weisman, R. B. *Science* **2002**, *298*, 2361−2366.

(40) Backes, C.; Schmidt, C. D.; Rosenlehner, K.; Hauke, F.; Coleman, J. N.; Hirsch, A. *Adv. Mater.* **2010**, *22*, 788−802.

(41) Bellare, J. R.; Davis, H. T.; Scriven, L. E.; Talmon, Y. *J. Electron Microsc. Technol.* **1988**, *10*, 87−111.

(42) Fantini, C.; Jorio, a.; Souza, M.; Strano, M.; Dresselhaus, M.; Pimenta, M. *Phys. Rev. Lett.* **2004**, *93*, 147406.

(43) Dresselhaus, M. S.; Dresselhaus, G. *Adv. Phys.* **2006**, *30*, 139−326.

(44) Cunha, J. R. A. D.; Fantini, C.; Andrade, N. F.; Alcantara, P.; Saraiva, G. D.; Filho, A. G. S.; Terrones, M.; Santos, M. C. D. *J. Phys. Chem. C* **2013**, *117*, 25138−25145.

(45) Leubner, S.; Katsukis, G.; Guldi, D. M. *Faraday Discuss.* **2012**, *155*, 253.

(46) Bartelmess, J.; Ehli, C.; Cid, J.-J.; García-Iglesias, M.; Vázquez, P.; Torres, T.; Guldi, D. M. *Chem. Sci.* **2011**, *2*, 652.

(47) Hohenester, U.; Goldoni, G. *Physics* **2011**, *4*, 5.

(48) Matsunaga, R.; Matsuda, K.; Kanemitsu, Y. *Phys. Rev. Lett.* **2011**, *106*, 037404.

(49) Park, J. S.; Hirana, Y.; Mouri, S.; Miyauchi, Y.; Nakashima, N.; Matsuda, K. *J. Am. Chem. Soc.* **2012**, *134*, 14461−14466.

(50) Nishihara, T.; Yamada, Y.; Okano, M.; Kanemitsu, Y. *Appl. Phys. Lett.* **2013**, *103*, 023101.

(51) Mouri, S.; Miyauchi, Y.; Iwamura, M.; Matsuda, K. *Phys. Rev. B* **2013**, *87*, 045408.

(52) Jakubka, F.; Grimm, S. B.; Zakharko, Y.; Gannott, F.; Zaumseil, J. *ACS Nano* **2014**, 8477−8486.

(53) Brozena, A. H.; Leeds, J. D.; Zhang, Y.; Fourkas, J. T.; Wang, Y. *ACS Nano* **2014**, 4239−4247.

(54) Rønnow, T. F.; Pedersen, T. G.; Cornean, H. D. *Phys. Lett. A* **2009**, *373*, 1478−1481.

(55) Oelsner, C.; Schmidt, C.; Hauke, F.; Prato, M.; Hirsch, A.; Guldi, D. M. *J. Am. Chem. Soc.* **2011**, *133*, 4580−4586.

(56) Richard, C.; Balavoine, F.; Schultz, P.; Ebbesen, T. W.; Mioskowski, C. *Science* **2003**, *300*, 775−778.

(57) Krieg, E.; Weissman, H.; Shirman, E.; Shimoni, E.; Rybtchinski, B. *Nat. Nanotechnol.* **2011**, *6*, 141−146.

(58) Krieg, E.; Albeck, S.; Weissman, H.; Shimoni, E.; Rybtchinski, B. *PLoS One* **2013**, *8*, e63188.

(59) Yang, K.; He, J.; Puneet, P.; Su, Z.; Skove, M. J.; Gaillard, J.; Tritt, T. M.; Rao, A. M. *J. Phys.: Condens. Matter* **2010**, *22*, 334215.

(60) Sweetman, L. J.; Nghiem, L.; Chironi, I.; Triani, G.; in het Panhuis, M.; Ralph, S. F. *J. Mater. Chem.* **2012**, *22*, 13800.

(61) Aldalbahi, A.; Panhuis, M. *Carbon* **2012**, *50*, 1197−1208.

(62) Pham, G. T.; Park, Y.-B.; Wang, S.; Liang, Z.; Wang, B.; Zhang, C.; Funchess, P.; Kramer, L. *Nanotechnology* **2008**, *19*, 325705.

(63) Park, J. G.; Smithyman, J.; Lin, C.-Y.; Cooke, A.; Kismarahardja, A. W.; Li, S.; Liang, R.; Brooks, J. S.; Zhang, C.; Wang, B. *J. Appl. Phys.* **2009**, *106*, 104310.

(64) Zhang, J.; Jiang, D.; Peng, H.-X.; Qin, F. *Carbon* **2013**, *63*, 125−132.